COMPUTATION OF THE WIGNER DISTRIBUTION FOR UNDULATOR RADIATION*

Ivan V. Bazarov and Andrew D. Gasbarro, CLASSE, Cornell University, Ithaca NY 14853 USA

Abstract

In the effort to optimize brightness in synchrotron radiation sources, questions arise as to the most desirable electron beam parameters given a particular insertion device. With a detailed understanding of the distribution of emitted photons, the electron beam profile can be effectively matched. We have developed tools which, by way of the Wigner distribution, compute the phase space of photons radiated by an electron bunch. An explanation is provided of the workings of the code itself with mention of important algorithms that have been implemented. We demonstrate via numerical examples the Wigner distributions of the undulator radiation. In particular, it is shown that the phase space of light differs appreciably from the Gaussian distribution assumed in many analytical expressions and, therefore, the more thorough approaches should be used for computation of related quantities.

WIGNER DISTRIBUTION

The application of the Wigner distribution function (WDF) to synchrotron radiation allows for phase space analysis of the x-ray fields. For a theoretical workup of the Wigner distribution function and its properties in this context, see [1, 2]. It has been demonstrated that the Wigner distribution, when properly normalized, gives the brightness of the classical geometrical ray corresponding to each point in phase space. Thus, the Wigner distribution and the brightness are simultaneously defined

$$\mathcal{B}(\mathbf{r}, \boldsymbol{\theta}) = \frac{I}{e} \frac{c\epsilon_0}{\pi\hbar\lambda^2} \int_{-\infty}^{\infty} d^2\mathbf{r}' \left\langle E^*(\mathbf{r} + \frac{\mathbf{r}'}{2})E(\mathbf{r} - \frac{\mathbf{r}'}{2}) \right\rangle e^{ik\mathbf{r}'\cdot\boldsymbol{\theta}}, \quad (1)$$

where $\mathbf{r}$ is the transverse displacement $\boldsymbol{\theta}$ is a vector of two angles giving the direction of the geometical ray. I is the average beam current , λ is the photon wavelength, and $< ... >$ denotes an ensemble average. Therefore, the Wigner distribution is the Fourier transform of the averaged autocorrelation-like function of the radiation fields (mutual optical intensity). In this work our aim is to demonstrate the numerical computation of the Wigner distribution.

Notice that the electric field here is scalar. In the case of vectorial fields of arbitrary polarization, the Wigner definition may be extended to form four separate distributions which are a generalization of Stokes' parameters. For computational examples of light with non-linear polarization

refer to [1]; here we limit our scope to linearly polarized light in x-direction.

An important quality of the Wigner is that is remains constant along phase space trajectories corresponding to classical drifts and lenses. Therefore, the distribution may be propagated via the simple matrix transformations from classical phase space optics.

Notice that for a radiation field on a grid detector, the Wigner distribution is a 4D quantity. While we have the ability to compute the full distribution, working with such an object numerically reaches limits of computer memory and CPU speed very quickly. Instead, we project this distribution into 2D $x - \theta_x$ phase space on which we perform the majority of our analysis.

NUMERICAL TOOLS

We have developed a suite of Matlab and C++ codes for numerically computing and analyzing the synchrotron radiation fields via the Wigner distribution function. In this section we provide a summary of various scripts and their roles in analysis.

Computing Radiation Fields

The first task in these evaluations is to produce a radiation field which is to be analyzed. For undulator radiation, the electron orbit is obtained using a symplectic integrator, from which the radiation fields are computed using well-known formulae. This program is written in C++ with parallel computing support for improved speed over Matlab (the language of choice for the rest of our scripts). A 2D rectangular grid detector is placed a distance z_0 from the center of the undulator. Its width and sampling rate may also be specified by the user along with all parameters necessary to specify the undulator itself. The ability to specify planar or helical undulators as well as segmented undulators separated by quadrupole magnets is included. The code also contains the ability to specify an arbitrarily defined magnetic field structure for more complex scenarios (e.g. introduction of misalignments of the electron orbit inside long segmented undulator).

As an alternative to synchrotron radiation fields, we have also written scripts which compute well-known Hermite-Gaussian and Laguerre-Gaussian laser modes, e_field_gauss_beam.m and e_field_lagauss_beam.m. These proved very useful for testing purposes allowing a direct comparison of WDF with analytical expressions.

Once fields are obtained, optional elliptical apodizing structures can be applied using aper.m. The "smooth-
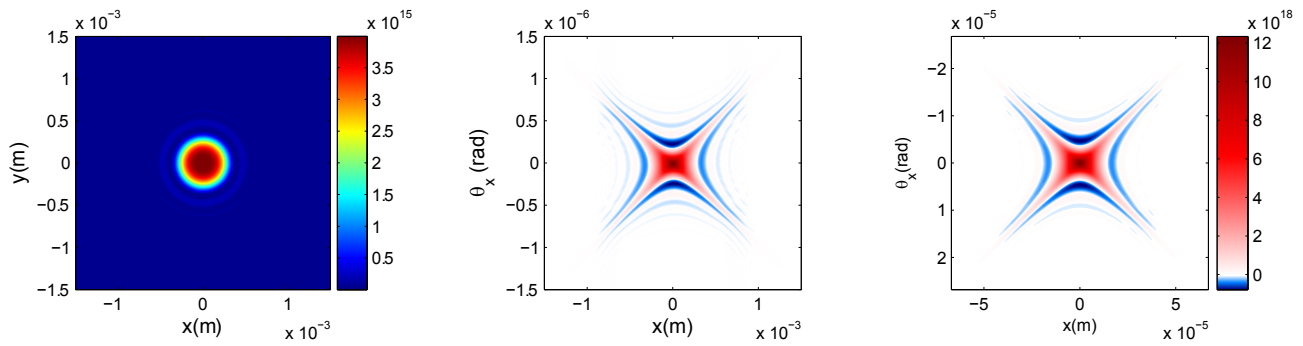
Figure 1: Left: Spatial flux density of radiation field. Center: Brightness at artificial waist. Right: Brightness at true waist. The flux density and 2D brightness are given in standard units: ph/(s 0.1%BW mm^2) and ph/(s 0.1%BW mm mrad) respectively.

ness" of these apertures may be modified, corresponding to a gaussian mask as opposed to a hard-edged screen.

Phase Space Analysis

The remaining Matlab scripts focus on numerical computation of the Wigner distribution and related quantities. The continuous Fourier transform in Eq. 1 is replaced with a discrete Fourier transform, and the computational challenge of the Wigner is reduced the finding the autocorrelation function. It is important that the grid spacing of the detector is fine enough to avoid aliasing effects. `wig2t.m` computes two dimensional $\theta_x - \theta_y$ cross sections at a specified point (x_0, y_0). The full 4D distribution is accessible via this function by finding 2D cross sections for each point on the detector grid. As we have mentioned, this is seldom a computationally feasible approach, so we favor computing 2D projected phase spaces using `wig2x.m`. The formulae for 2D projected WDFs is given in [1].

Once the Wigner is found, we have the ability to apply drifts and thin lenses to the distribution using `wigner_drift.m` and `wigner_lens.m`. Again, these transformations are the same simple transformations performed on classical phase spaces. Drifts and lenses may also be applied to the radiation field in principle, however, this is a more complicated operation (we only apply a thin lens to the field at one point in the Wigner computation using `e_field_flatten_phase.m` to avoid aliasing for convenient grid sizes – this procedure is demonstrated in a numerical example below).

The mutual optical intensity can be obtained either directly from the synchrotron radiation fields or via the Wigner distribution by a Fourier transform. `moi2.m` finds this quantity while `cdc2.m` computes the complex degree of coherence, which is simply the normalized mutual optical intensity and the quantity directly related to the fringe visibility in Young's double-slit experiment.

The WDF may take on negative values, yet it can still act as a quasi-probability distribution function when normalized to 1. `emit.m` computes the sigma matrix, Σ, the Twiss parameters and the emittance, ϵ, of this normalized distribution. In an example below, we demonstrate how the
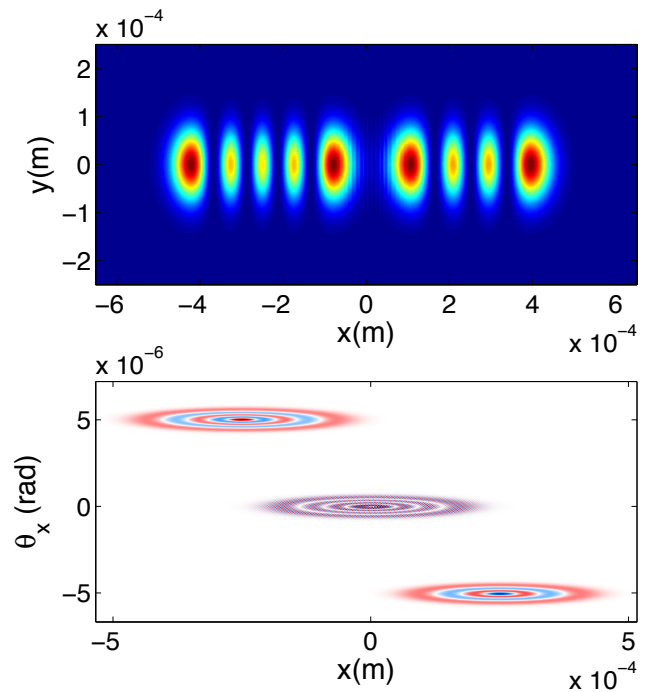

Figure 2: Spatial flux density (top) and brightness (bottom) of $H_{tot} = H_{3,0} + H_{4,0}$. The color maps are similar to Figure 1

emittance and beta-function of synchrotron radiation differ from commonly cited values.

`A_Brightness.m`, `A_Brightness2D.m`, `A_Flux.m`, and `A_SpatialFluxDensity.m` compute the 4D peak brightness, 2D peak brightness, integrated flux, and spatial flux density as cited in well known analytical formulae [3]. Demonstration of agreement between analytical and numerical computation of these quantities has been shown in [1].

NUMERICAL EXAMPLES

Here we provide three examples of numerical analysis performed using the aforementioned computational tools.

Table 1: Undulator, Beam, and Radiation Parameters

Number of Periods	N_u	250
Undulator Length	λ_u	2 cm
Photon Energy	E_{ph0}	7.915 keV
Beam Energy	E	5 GeV
Average Current	I	100 mA
Detector Position	z_0	50 m

In the first example, we show the steps in computing the WDF for on resonance undulator radiation back-propagated to the undulator center. First the radiation field is computed using the parameters specified in Table 1. After a certain drift to the detector (50 m in this case), the radiation pattern is obtained on the rectangular grid. The quadradic phase factor is removed from the field using `e_field_flatten_phase.m`, which is equivalent to applying a thin lens which "flattens" the phase space and creates an artificial waist. This helps to avoid aliasing problems in WDF as mentioned previously. It is here that the phase space is first be computed. Once the Wigner distribution is obtained at the artificial waist, it is easy to remove the phase-flattening lens using `wigner_lens.m` and then back-propagate the phase space to the undulator center, which is also equivalent to 1:1 focusing of the undulator source. The process is shown in Figure 1.

For the second example, we demonstrate the coherent addition of two Hermite-Gaussian modes in phase space. The superposition is an equally weighted sum of $H_{3,0}$ and $H_{4,0}$, where $H_{m,n}$ is a Hermite-Gauss mode of order m in x and order n in y. The $H_{3,0}$ laser is offset with $(x_{\mathrm{ini}}, \theta_{x,\mathrm{ini}}) = (0.25\,\mathrm{mm}, -5\,\mu\mathrm{rad})$. The $H_{4,0}$ laser is offset with $(x_{ini}, \theta_{x,ini}) = (-0.25\,\mathrm{mm}, 5\,\mu\mathrm{rad})$ The radiation field is then simply $H_{\mathrm{tot}} = H_{3,0} + H_{4,0}$. Figure 2 shows the radiation pattern at the detector and the phase space at the waist. Notice the interference term that forms from the coherent superposition of the radiation fields. It is the disappearance of this term that leads to loss of coherence in radiation.

As a final demonstration, we examine how the values of the emittance and betatron function change with the flux fraction. The radiation field is the same undulator radiation pattern used for Example 1 (Table 1). The effect is shown in Figure 3. For each point on the plot, an ellipse of fixed area is fit over the phase space in such a way that the flux contained inside the ellipse is maximized; all points outside the ellipse are thrown away and the emittance and betatron function are computed for the remaining points. From right to left, the ellipse area decreases from an all-encompassing ellipse to an ellipse of zero area. The horizontal dotted lines show the commonly cited values for the betatron function, $\beta = L_u/2$ and $\beta = L_u/2\pi$ (L_u is the undulator length). The emittance of undulator radiation is typically assumed to be the diffraction limited value, $\epsilon = \lambda/4\pi$. Not only do the values of emittance and the betatron function differ from commonly cited values for the entire radiation flux,
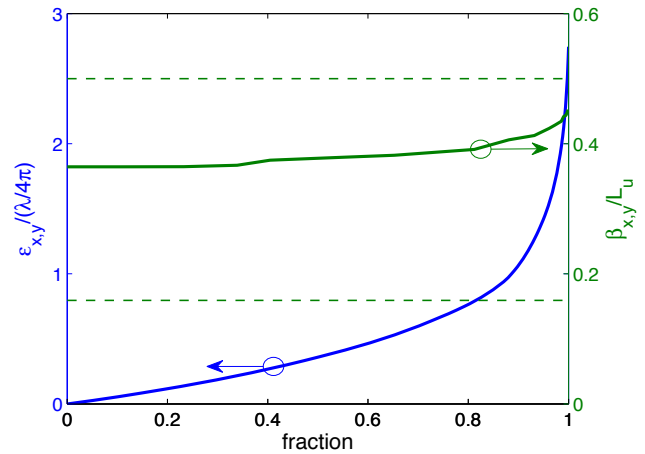
Figure 3: Emittance and betatron function vs fraction.

but they also vary significantly with fraction. This analysis suggests a much more careful handling of these values, especially for electron beam matching and undulator design.

ACCOUNTING FOR FINITE BUNCH

All analysis so far has been for a single electron, and convolution to many electrons comes with some challenges even though straightforward in every other aspect [1, 2]. The situation becomes particularly simple when offsetting electrons in x_{ini} and $\theta_{x,\mathrm{ini}}$ which does nothing but shift the center of the Wigner distribution (the case of infinitely wide in x planar undulator). However, spatial offsets in y may change the effective K-parameter of the undulator due to the cosh-like dependence of the magnetic field strength on y [1]. This causes an effective resonance wavelength shift of

$$\lambda_{\mathrm{res}} - \lambda_{\mathrm{res0}} = \frac{\lambda_u k^2}{4\gamma^2}(\cosh^2(\frac{2\pi}{\lambda_u} y_{\mathrm{ini}}) - 1). \quad (2)$$

which can be adjusted for in the case of small offsets. λ_{res} is the new resonant wavelength, λ_{res0} is the on axis resonant wavelength, and λ_u is the undulator wavelength. Large offsets in $\theta_{y,ini}$ must be treated even more carefully as the effective K-parameter varies along the electron path. Other important effects arise from the nonzero energy spread in the electron bunch, see [1].

In summary, the effort to analyze realistic sources using the Wigner distribution and phase space techniques has only just begun. We expect that this method will grow in importance with the advent of more coherent light sources.

REFERENCES

[1] Ivan V. Bazarov. Synchrotron radiation representation in phase space. *PRSTAB*, 15:050703, May 2012.

[2] Kwang-Je Kim. Brightness, coherence and propagation characteristics of synchrotron radiation. *NIMA A*, 246(1-3):71 – 76, 1986.

[3] Kwang-Je Kim. Characteristics of synchrotron radiation. *AIP Conf. Proc.*, 184(1):565–632, 1989.